Supporting information

In vivo Aggregation-Induced Transition between T_1 and T_2 Relaxations of Magnetic Ultra-Small Iron Oxide Nanoparticles in Tumor Microenvironment

Huige Zhou [1], Jinglong Tang [1], Jiayang Li, Wanqi Li, Ying Liu, Chunying Chen *

Author contributions

H. Z. and J. T. designed and performed the experiments, collected and analyzed the data and co-wrote the manuscript. C. C. conceived the principal idea, designed the experiments and wrote the manuscript. J. L., W. L. and Y. L. interpreted the data and provided advice. All the authors discussed the results and commented on the manuscript.

CAS Key Laboratory for Biomedical Effects of Nanomaterials and Nanosafety, & CAS Center for Excellence in Nanosciences, National Center for Nanoscience and Technology of China
No.11 Beiyitiao, Zhongguancun, Beijing 100190, P.R. China

[1] These authors contributed equally to this work.

*Corresponding authors.

Tel: +86 10 82545560; fax: +86 10 62656765

E-mail address: chenchy@nanoctr.cn

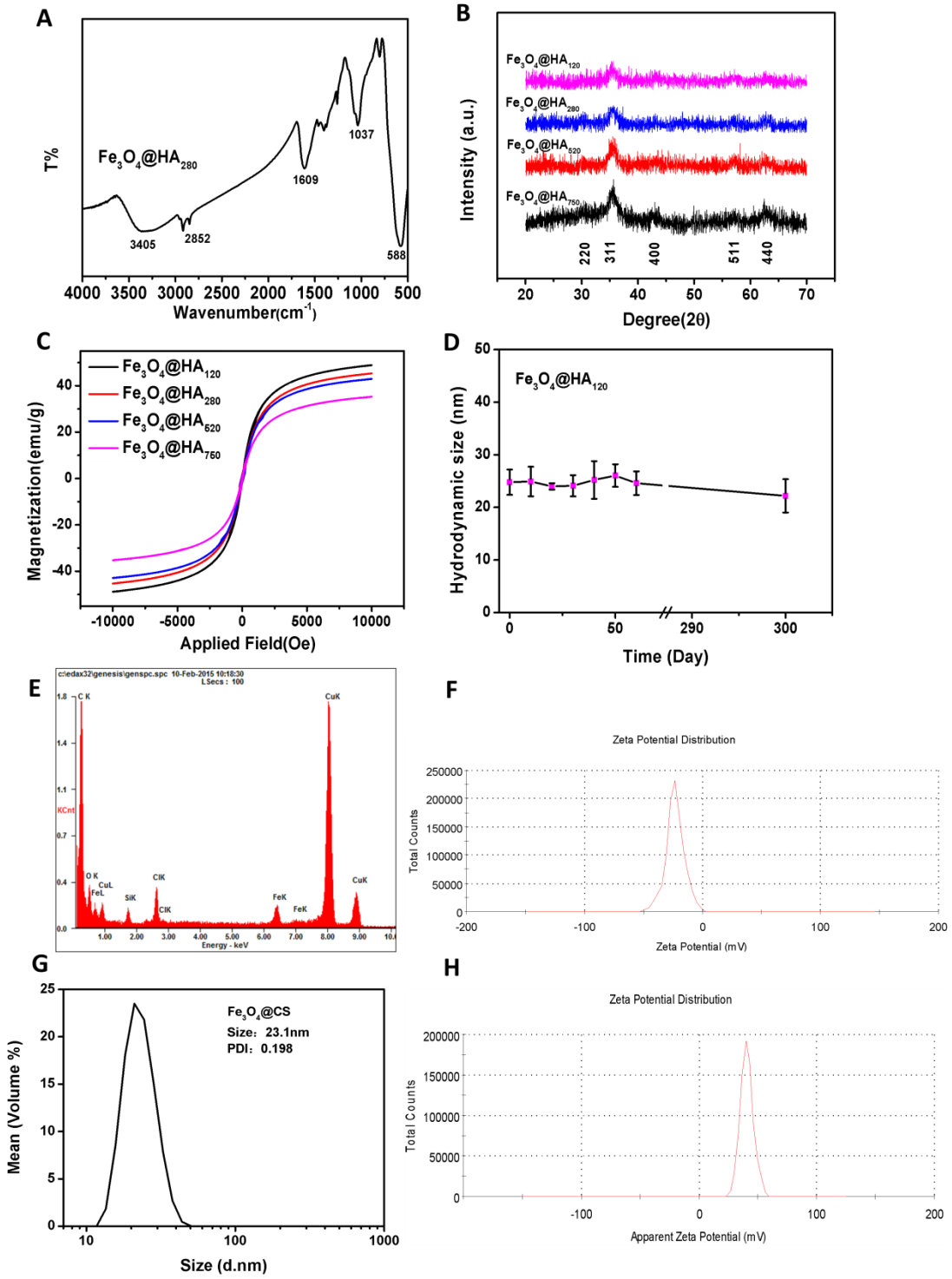

Figure S1. (A) FT-IR spectrum of Fe_3O_4@HA_{280}; (B) X-ray diffraction patterns and (C) Field-dependent magnetization curve of Fe_3O_4@HA at room temperature (emu per gram of Fe_3O_4); (D) colloid stability; (E) EDX spectrum and (F) Zeta potential distribution of Fe_3O_4@HA_{280}; (G) Hydrodynamic size distribution and Zeta potential of Fe_3O_4@CS.

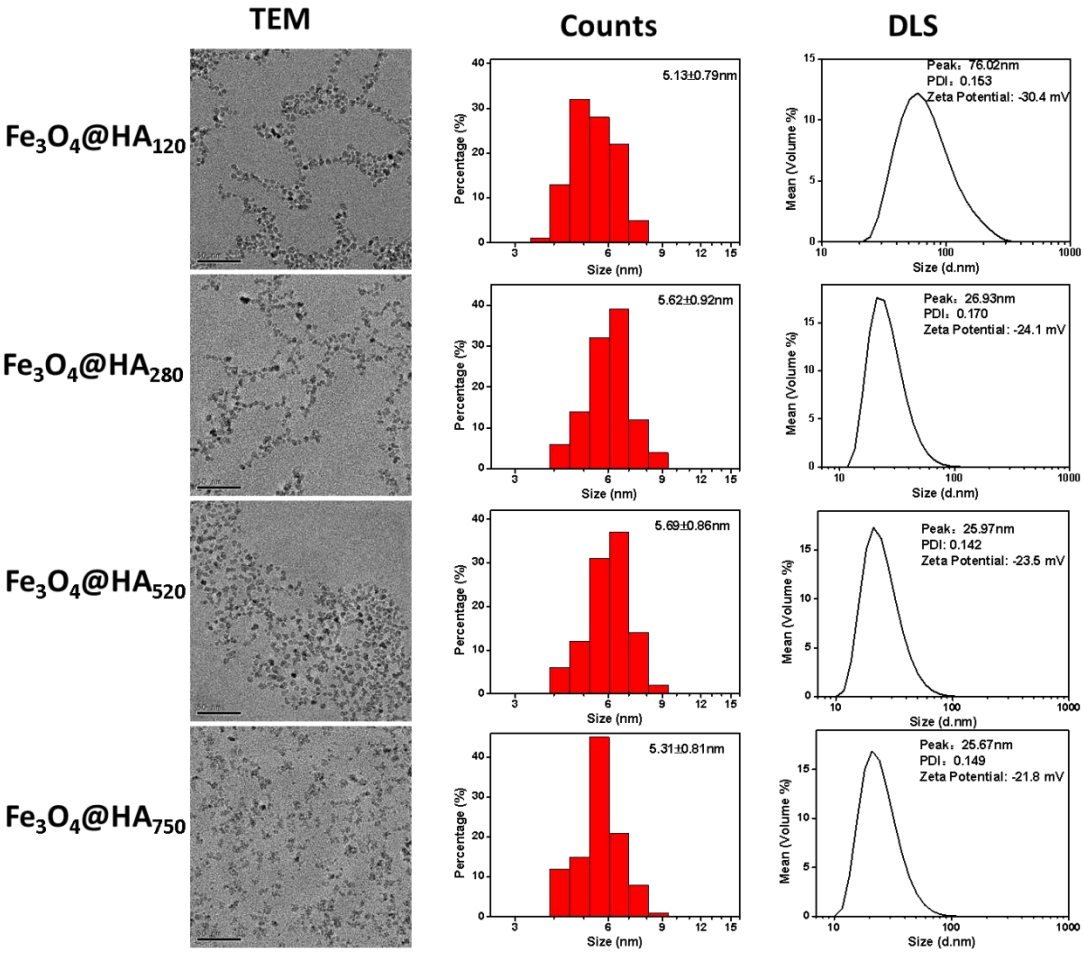

Figure S2. Size distribution of Fe_3O_4@HA nanoparticles, TEM images, diameter statistics (Image J) and hydrodynamic size distribution, scale bar = 50 nm.

Table S1. Reported r_1 and r_2 value of various nanoparticles.

Surface ligand	Size (nm)	r_1(mM^{-1}s^{-1})	r_2(mM^{-1}s^{-1})	Magnetic field	Reference
PO-PEG	2.2	4.78	17.5	3.0 T	[1]
PO-PEG	3	4.77	29.2	3.0 T	[1]
PO-PEG	12	2.37	58.8	3.0 T	[1]
PMAA-PTTM	3.3	8.30	35.1	4.7 T	[2]
PAA	1.7	8.20	16.7	1.4 T	[3]
PAA	2.2	6.15	28.6	1.4 T	[3]
PAA	4.6	1.06	64.4	1.4 T	[3]
DP-PEG	3.6	3.21	24.6	3.0 T	[4]
DP-PEG	10.9	3.24	79.1	3.0 T	[4]
CSQ	11.9	1.18	440.6	7.0 T	[5]
Gd-DTPA		4.80	5.3	4.7 T	[2]
SHU-555C		2.90	69.0	4.7 T	[2]

Table S2. The calculation process of the number of HA on the surface of one iron oxide nanoparticles.*

	Fe_3O_4@HA_{120}	Fe_3O_4@HA_{280}	Fe_3O_4@HA_{520}	Fe_3O_4@HA_{750}
Input HA (g)	0.25	0.5	1	2
Diameter of Fe_3O_4 core (nm)	5.13	5.62	5.69	5.31
Radius of Fe_3O_4 core (nm)	2.55	2.80	2.85	2.65
Volume of Fe_3O_4 core (nm)	69.4	92.0	97.0	78.0
$Mass_1$ of Fe_3O_4 core (g, $\times 10^{-21}$)	380	476	502	404
$Mass_2$ of total material (mg)	6.15	8.20	12.4	17.9
$Mass_3$ of Fe (mg)	0.959	0.770	0.649	0.591
$Mass_4$ of Fe_3O_4 (mg)	1.33	1.06	0.896	0.816
Ratio (Fe_3O_4/ total material, %)	21.55	12.97	7.23	4.55
$Mass_5$ of Fe_3O_4 core (g)	0.216	0.130	0.0790	0.0455
$Mass_6$ of HA (g)	0.785	0.870	0.921	0.954
Number (Fe_3O_4) ($\times 10^{17}$)	5.99	2.72	1.58	1.13
Number (HA) ($\times 10^{19}$)	6.95	7.72	8.15	8.45
Number of HA on one core	～120	～280	～520	～750
Surface density of HA (mg/m^2)	～32	～65	～126	～193

***** Diameter of core was measured by the counts of Image J from TEM images (Fig S2); radius of core was half of diameter; core volume was given by the volume formula for sphere ($4/3\pi r^3$); $mass_1$ of core was acquired by: $4/3\pi r^3 \times \rho(Fe_3O_4)$ ($\rho(Fe_3O_4) = 5.18\ gcm^{-3}$); mass of total materials and iron were obtained by lyophilization and ICP-OES respectively; mass of Fe_3O_4 were obtained by: $Mass\ (Fe) \times M(Fe_3O_4)/(3 \times M(Fe))$ ($M(Fe_3O_4) = 231$, $M(Fe) = 56$); ratio of Fe in total materials was obtained by mass (Fe_3O_4)/ mass (total material); $mass_5$ of core (g) and $mass_6$ of HA (g) was calculated from the ratio of Fe_3O_4 in one gram materials; number of core was acquired by $mass_5/mass_1$; number of HA was gotten by $Mass_6 \times N_A/M_w$, where N_A is avogadro's constant and $N_A = 6.02 \times 10^{23}, M_w = 6800$; number of HA on one core was calculated by: Number (HA)/Number (Fe_3O_4).

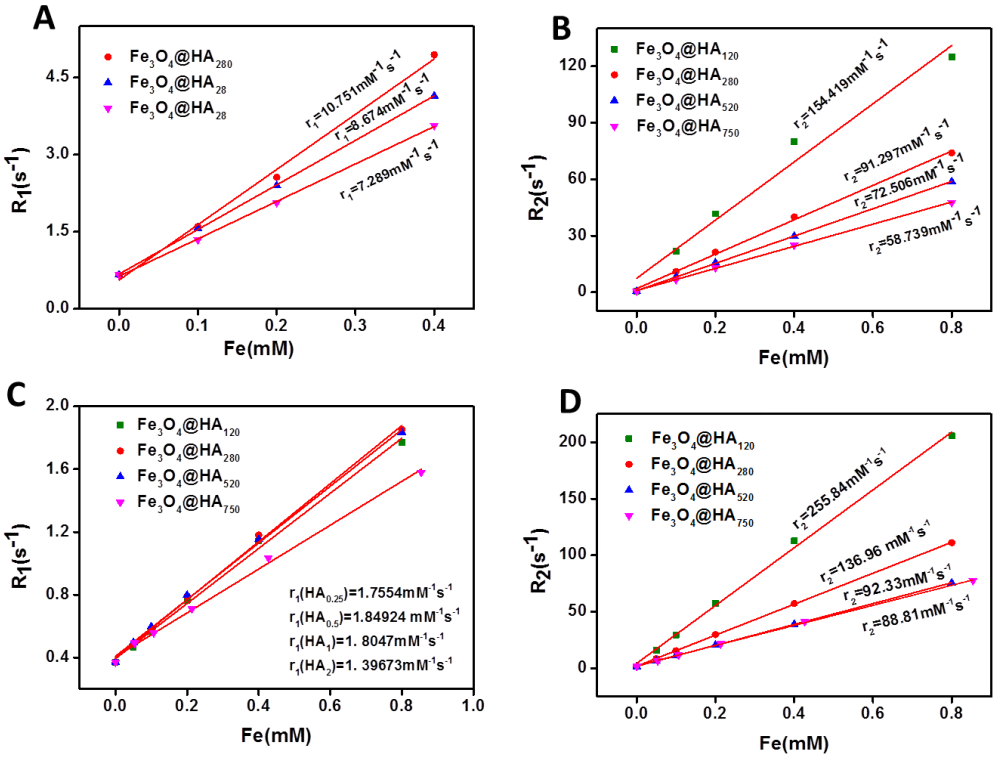

Figure S3. Plots of R_1 (A, C) and R_2 (B, D) versus Fe concentration of Fe_3O_4@HA at different applied magnetic fields (A, B: 3 T; C, D: 7 T).

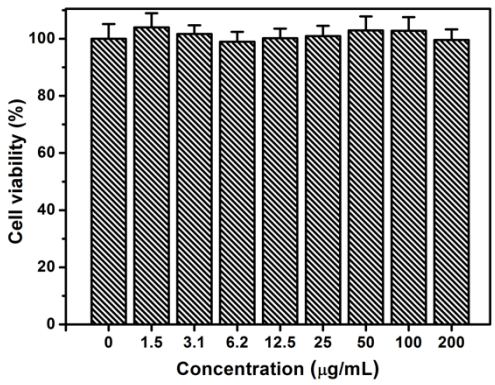

Figure S4. Viability of MDA-MB-231 cells after incubation with various iron concentrations of Fe_3O_4@HA_{280} for 24 h (n = 5).

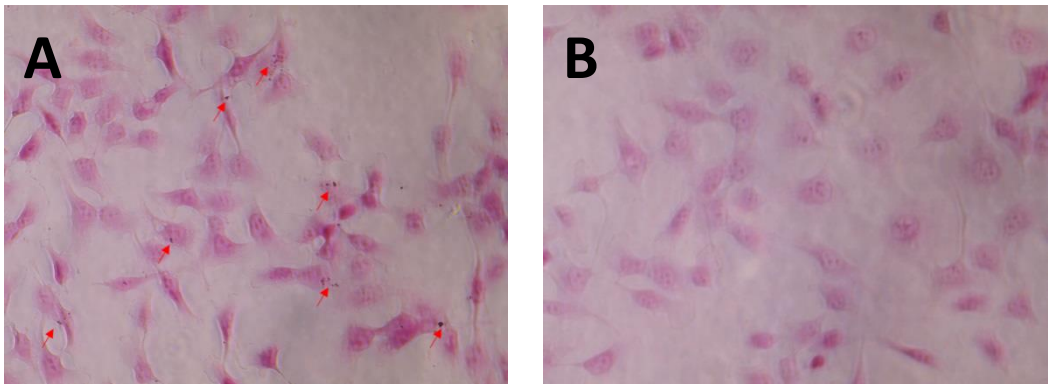

Figure S5. *In vitro* Prussian blue staining images of MDA-MB-231 cells after 24 h treatment with Fe_3O_4@HA_{280}, without (A) or with (B) free HA competition.

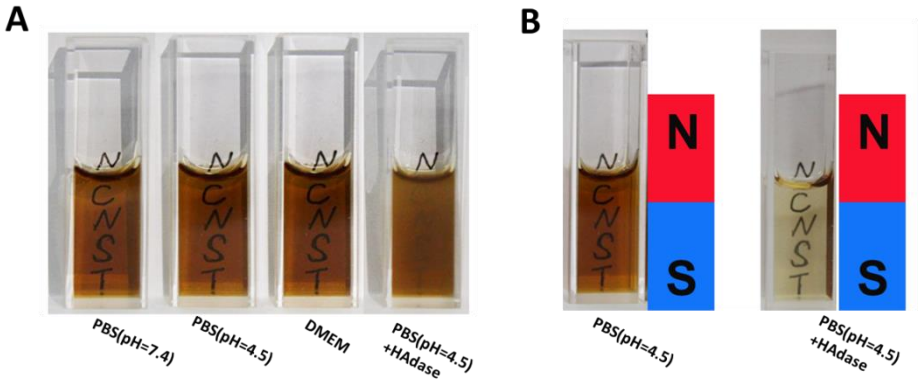

Figure S6. (A) Colloid stability of Fe_3O_4@HA_{280} in different environments; (B) Photos of Fe3O4@HA280 in pH 4.5 PBS solutions in the absence and presence of HAdase in a magnetic field.

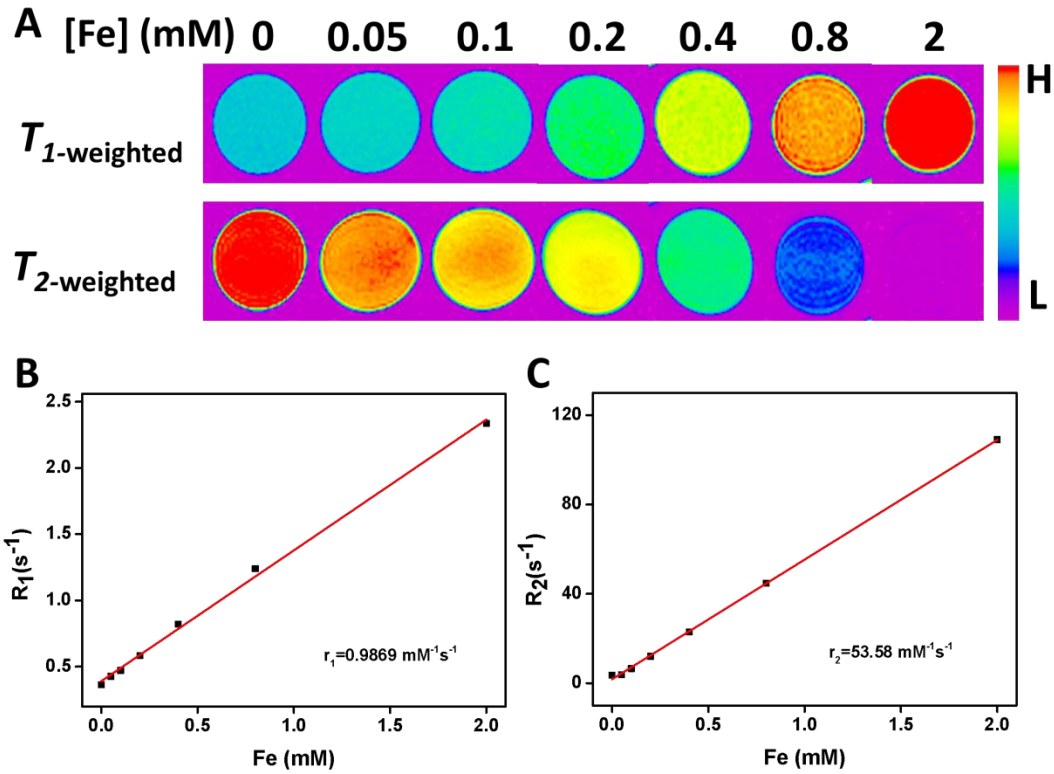

Figure S7. (A) T_1 and T_2 weighted MR images and (B) Plots of R_1 (B) and R_2 (C) versus Fe concentration of Fe_3O_4@CS at 7 T applied magnetic fields.

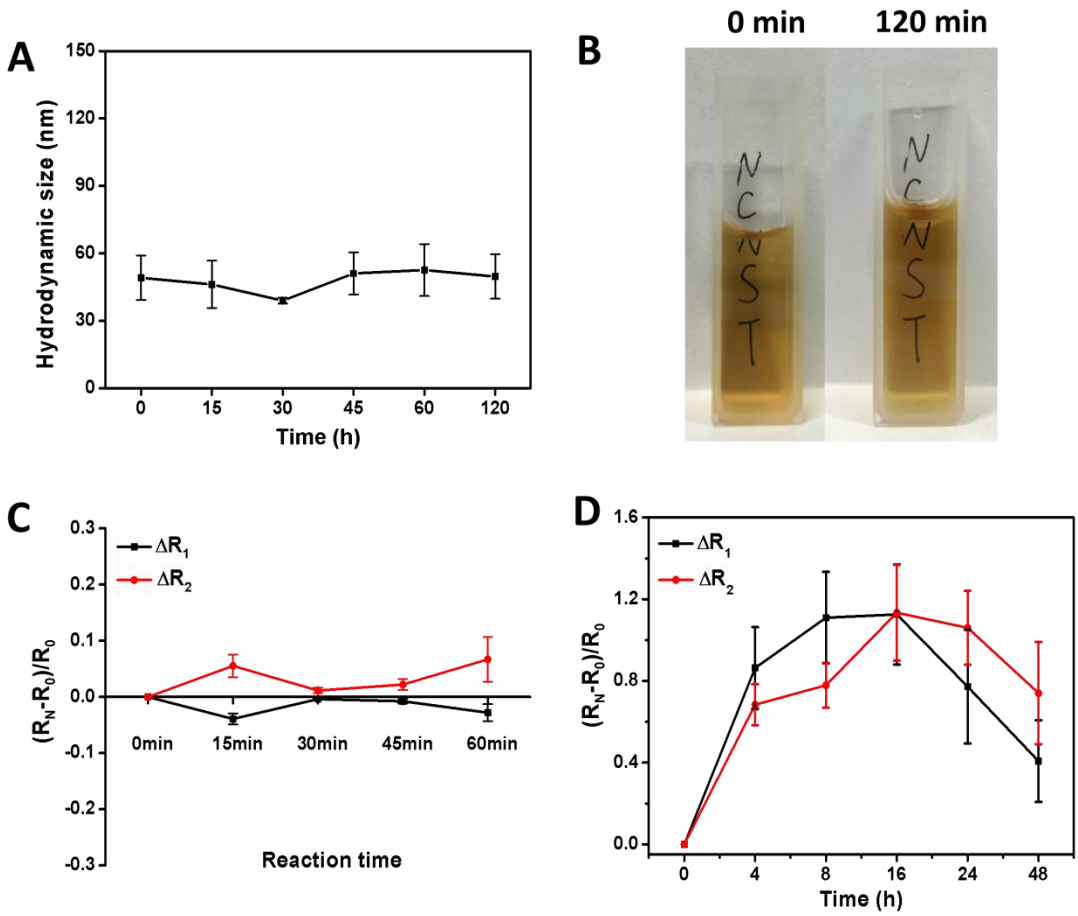

Figure S8. (A) Hydrodynamic size and (B) Colloid stability of Fe_3O_4@CS in pH 4.5 at different time points in the presence of HAase (37 °C water bath). R_1 and R_2 changes of Fe_3O_4@CS in PBS (pH 4.5) under the presence of HAdase (C) and in MDA-MB-231 cells (20 μg Fe/mL) (D), R_0 represent R_1 or R_2 at 0 min and R_N represents R_1 or R_2 at the following time point. (n = 3)

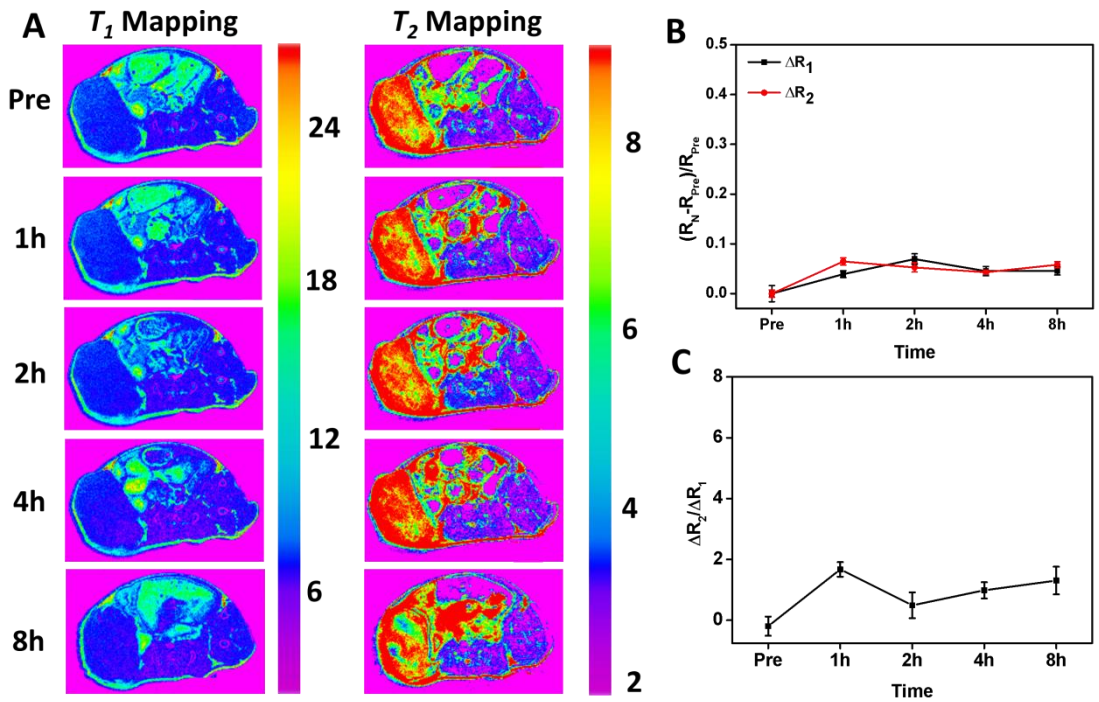

Figure S9. (A) T_1 and T_2 MRI mapping of the nude mouse bearing tumor before and at 1 h, 2 h, 4 h and 8 h after intravenous injection of Fe_3O_4@CS (2.5 mg Fe/kg). (B) Results from the analyses of T_1/T_2 maps; (C) $\Delta R_2/\Delta R_1$ ratio of the left images. Only the region of interest comprising the tumor was considered for the analysis.

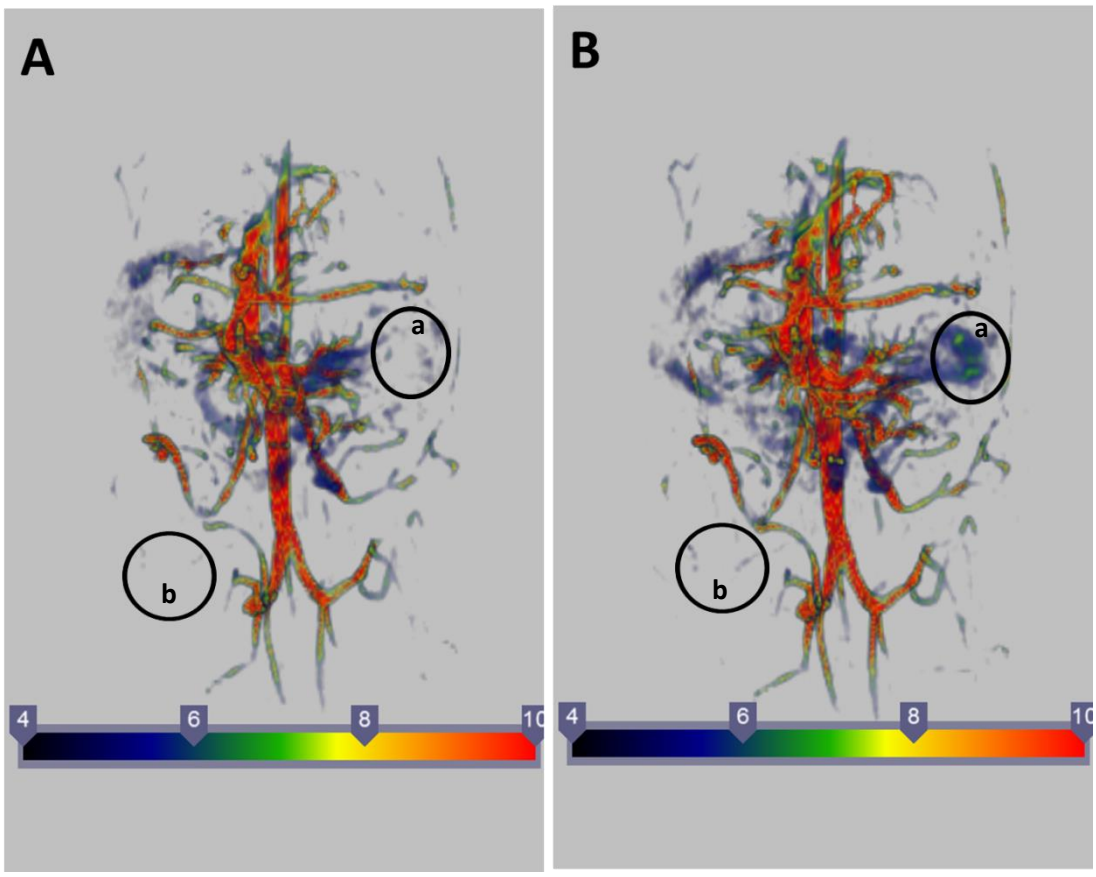

Figure S10. Enhanced high-resolution blood pool MR images obtained using 3d-FLASH sequence (A) Before- and (B) After-injection Fe_3O_4@HA_{280}. Blood pool MR images of kidney (a) and tumor (b).

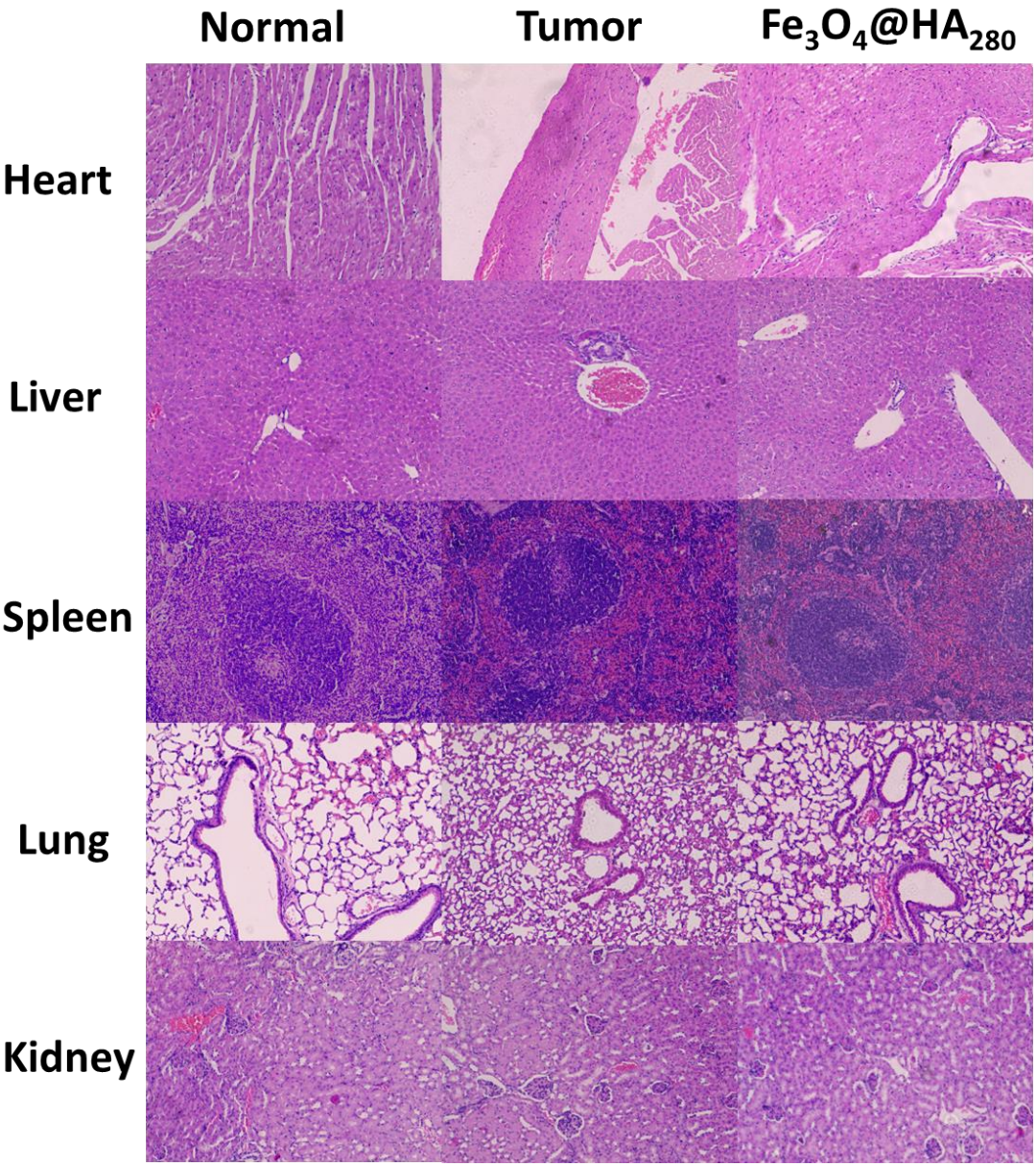

Figure S11. H&E staining of tissue from selected organs harvested at 48 h for normal nude mouse and nude mouse bearing tumor after the injection of PBS, and 2.5 mg Fe/kg of Fe_3O_4@HA_{280}.

The theoretical derivation of the relationship of solution viscosity and r_1

According to the USPIO relaxation mechanism, the outersphere contribution to the relaxation is dominant as compared to the innersphere contribution which is so minor that can be completely negligible.[6] With the boundary conditions of high magnetic field, r_1 and r_2 can be given by[4, 7, 8]

$$r_1 = \frac{128\pi^2\gamma_I^2 M_n}{405\rho}\left(\frac{1}{1+L/a}\right)^3 M_s^2\tau_D J_A\left(\sqrt{2\omega_1\tau_D}\right) \quad \text{(S1)}$$

$$r_2 = \frac{256\pi^2\gamma_I^2 M_n}{1215\rho}\left(\frac{1}{1+L/a}\right)^3 M_s^2\tau_D \quad \text{(S2)}$$

In equation (1) and equation (2), γ_I is the proton gyromagnetic ratio, M_n, ρ and are the molar mass, density of Fe_3O_4, a and M_s are the radius and saturation magnetization of the Fe_3O_4 core, L is the water impermeable thickness of the particles, r is the effective radius of particles ($r = L + a$), J_A is Ayant's density spectral function:

$$J_A(z) = \frac{1+\frac{5z}{8}+\frac{z^2}{8}}{1+z+\frac{z^2}{2}+\frac{z^3}{6}+\frac{4z^4}{81}+\frac{z^5}{81}+\frac{z^6}{648}} \quad \text{(S3)}$$

Where $z = \sqrt{2\omega_I\tau_D}$, ω_I is the proton Larmor frequency, which is only determined by the applied magnetic field (3 T: 128 MHz; 7 T: 400 MHz). τ_D is the translational diffusion time and it can be given by[6]

$$\tau_D = \frac{r^2}{D} \quad \text{(S4)}$$

Our Fe_3O_4@HA nanoparticles were in a colloid system, and in this system, can be given by Stokes-Einstein equation:

$$D = \frac{kT}{6\pi\eta r^2} \quad \text{(S5)}$$

Then, we can get from equation (S4) and equation (S5)::

$$\tau_D = \frac{6\pi\eta r^3}{kT} \quad \text{(S6)}$$

In the above equations, is the water diffusion coefficient, k is Boltzmann constant, T is temperature, η is the viscosity of the solution, r is the particle radius.

In polymer solution, η can be given by:

$$\frac{\eta - \eta_0}{\eta_0} = \eta_{sp} \quad \text{(S7)}$$

$$\eta_{sp} = [\eta]c + k'[\eta]^2 c^2 \quad \text{(S8)}$$

Where η_0 is the viscosity of the solvent, $[\eta]$ and η_{sp} are the intrinsic viscosity and specific viscosity of polymer solution, c is the concentration of polymer, k' is Huggins parameter. k' equal to 0.3～0.4 when the system is linear flexible polymer chain segment and its good solvent. HA is linear chain polymer, and dissolve well in water, so it has a positive Huggins parameter.

The water impermeable thickness of Fe_3O_4@HA_{120} is similar with the others for the molecular semi-rigid of HA in water[9] and the loosen clusters could be penetrate by water molecular. Since the size of magnetic core and the water impermeable thickness are similar for Fe_3O_4@HA_{120}, Fe_3O_4@HA_{280}, Fe_3O_4@HA_{520} and Fe_3O_4@HA_{750}, the different parameter in equation S1&S2 for these four kinds of nanoparticles is M_s and τ_D.

$\tau_D J_A$ is more important for r_1 than M_s because of the non-monotonic variation against τ_D. As shown (Figure S5A), the value of $\tau_D J_A$ in 3 T magnetic field is greater than in 7 T and when the applied magnetic field is 7 T,

it changes little. This trend is similar with the trend of r_1 values of iron oxide with increasing density of HA surface ligand. Then, it can be speculated that HA density on one nanoparticles and τ_D may have some relationship.

Since these nanoparticles can be considered as a colloid system, they can be connected by the Huggins equation (S5). Then, it can be deduced that when the density of surface ligand increase, the concentration of HA in aqueous is increasing with the same amount of Fe_3O_4. According to equation (S7) and equation (S8), the viscosity of the solution is increasing following the growth of HA, so the translational diffusion time τ_D is increase (as shown in Figure S5B). There will be a peak value since $\tau_D J_A$ increase first and then decrease. The variation trend of r_1 values at 7 T and 3 T agrees well with the trend of $\tau_D J_A$ as the increase density of surface ligand. Therefore, we think this explanation is reasonable.

Supporting references

1. B. H. Kim, N. Lee, H. Kim, K. An, Y. I. Park, Y. Choi, K. Shin, Y. Lee, S. G. Kwon, H. B. Na, J. G. Park, T. Y. Ahn, Y. W. Kim, W. K. Moon, S. H. Choi and T. Hyeon, *J. Am. Chem. Soc.*, 2011, **133**, 12624-12631.
2. Z. Li, P. W. Yi, Q. Sun, H. Lei, H. L. Zhao, Z. H. Zhu, S. C. Smith, M. B. Lan and G. Q. Lu, *Adv. Funct. Mater.*, 2012, **22**, 2387-2393.
3. G. N. Wang, X. J. Zhang, A. Skallberg, Y. X. Liu, Z. J. Hu, X. F. Mei and K. Uvdal, *Nanoscale*, 2014, **6**, 2953-2963.
4. J. F. Zeng, L. H. Jing, Y. Hou, M. X. Jiao, R. R. Qiao, Q. J. Jia, C. Y. Liu, F. Fang, H. Lei and M. Y. Gao, *Adv. Mater.*, 2014, **26**, 2694-2698.
5. H. Zhou, X. Hou, Y. Liu, T. Zhao, Q. Shang, J. Tang, J. Liu, Y. Wang, Q. Wu, Z. Luo, H. Wang and C. Chen, *ACS Appl. Mat. Interfaces*, 2016, **8**, 4424-4433.
6. S. Laurent, D. Forge, M. Port, A. Roch, C. Robic, L. V. Elst and R. N.

Muller, *Chem. Rev.*, 2008, **108**, 2064-2110.

7. A. Roch, R. N. Muller and P. Gillis, *J. Chem. Phys.*, 1999, **110**, 5403-5411.
8. R. N. Muller, L. Vander Elst, A. Roch, J. A. Peters, E. Csajbok, P. Gillis and Y. Gossuin, *Adv. Inorg. Chem.*, 2005, **57**, 239-292.
9. M. K. Cowman and S. Matsuoka, *Carbohydr. Res.*, 2005, **340**, 791-809.